# Multiorder Sequential Joint Inversion of Gravity Data With Inhomogeneous Depth Weighting: From Near Surface to Basin Modeling Applications

Luigi Bianco, Mojtaba Tavakoli, Andrea Vitale, and Maurizio Fedi

***Abstract*— We have established a workflow for a multiorder sequential joint inversion (MOSJI) of gravity and gravity gradients, that aims at modeling vertically stacked sources in various geological scenarios. We consider the joint inversion of the gravity data and one of the *h*th-order derivatives of the gravity data. The first step involves separate inversions, which are fundamental to fully exploit the different wavelength-content of the two quantities to invert. The joint inversion is warranted by using the scheme of a sequential joint inversion with a cross-gradient constraint. The algorithm is able to exploit different types of a priori information, such as compactness and inhomogeneous model-weighting function. First, we test this approach on a realistic synthetic model from the SEg Advanced Modeling (SEAM) Phase I model, involving salt and mother salt structures. Then, we consider a synthetic model containing either shallower or deeper karst cavities. These tests produced a better modeling of both shallower and deeper sources, when compared to the separate unconstrained inversions. Thanks to these good results, we apply our method to a real case for cavity detection in Southern Spain. The method shows an accurate modeling of the expected sources. In all the aforementioned tests, we obtain a strong decrease of the cross-gradient values and a meaningful linearization in the scatter plots of physical parameters, both indicating the good performance of the joint inversion.**

***Index Terms*— Cross-gradient, gravity, gravity gradients, joint inversion, near-surface, salt modeling, workflow.**

## I. Introduction

GRAVITY field has been widely used in geophysics in different scenarios, from exploration to natural hazards. The interpretation of these data may benefit from additional information brought from the gravity gradient tensor (GGT) measurements. In a Cartesian system, GGT is expressed as the second-order derivatives of the Earth's gravitational potential components in $x$-, $y$-, and $z$- directions. Since the late 1700s, gradients of gravity field have been acquired [1] and the vertical gradient [2] has been geologically interpreted to estimate the density-contrasts of underground bodies such as salt domes, ores, cavities, and others.

With modern technology derived from military applications [3], the opportunity to measure the GGT components has represented a significant improvement compared to the gravity survey, where only the vertical component of the field ($G_z$) is acquired. Gravity and gravity gradient decay in a different way and therefore are characterized by different wavelength content, thus being more sensitive to deep or shallow sources, respectively.

These datasets are interpreted by forward modeling or inversion. However, we must deal with the inherent non-uniqueness of the solution. Geophysicists face this type of problem introducing a priori information such as a geological knowledge of the area or interpretation of the subsurface coming from other methodologies. Another way to decrease ambiguity is to invert different datasets at the same time. In this framework, we could invert single components of the GGT (i.e.: $G_{zz}$) or combinations of them [4], [5], [6]. Different authors have explored these opportunities. Biegert et al. [7] found that $G_z$ and GGT inversion could be used to define the thickness of the salt and its top, respectively. Capriotti and Li [8] developed an algorithm to jointly invert $G_z$ and GGT adopting a unique data misfit. They achieved improved solutions at depth when compared to inverting only the gravity gradient data for a simple block and a basin-like test. Paoletti et al. [9] performed a joint inversion on the Vredefort Crater and analyzed its performance through a singular value analysis. They found that GGT does not improve the resolution of inverted models, these last not depending on the used components.

These results agree with the findings by Ialongo et al. [10], who analyzed separate inversion of a target source and found an invariant behavior of the models retrieved from different $h$-order derivatives of the potential field. However, some loss of resolution occurred in deeper layers suggesting that we should prefer a low-order differentiation to retrieve better information at depth. Capriotti and Li [11] jointly inverted gravity and gravity gradient fitting each dataset at its own noise level. They adopted a weighting parameter among the different parts of an enlarged data misfit and obtained improved models in basin-like tests.

Although the actual improvement brought by jointly inverting gravity and gravity gradients data is still debated, we can address this topic by looking at both the positive and negative

Manuscript received 20 April 2023; revised 11 August 2023 and 16 October 2023; accepted 4 December 2023. Date of publication 6 December 2023; date of current version 18 December 2023. *(Corresponding author: Luigi Bianco.)*

Luigi Bianco and Maurizio Fedi are with the Department of Earth, Environment and Resources Sciences, University of Naples "Federico II," 80126 Naples, Italy (e-mail: luigi.bianco2@unina.it; fedi@unina.it).

Mojtaba Tavakoli is with the Khorasan Razavi Gas Company, Ershad Boulvard, 9185837755 Mashhad, Khorasan Razavi, Iran.

Andrea Vitale was with the Institute for Electromagnetic Sensing of the Environment, National Research Council, Naples, Italy. He is now with the Institute for Agriculture and Forestry Systems in the Mediterranean, National Research Council, 80055 Naples, Italy.

Digital Object Identifier 10.1109/TGRS.2023.3340037

findings mentioned before. In fact, we can consider the results of Capriotti and Li [11] as an opportunity to get different information from different orders of vertical derivatives.

In order to fully exploit the different wavelength contents of these datasets, we have to find an appropriate strategy to not combine all the data in a unique data misfit. This leads to the strategy of treating them as two separate datasets and combining resulting models via a structural constraint called cross-gradient constraint. The cross-gradient constraint was first introduced by Gallardo and Meju [12] and has been applied to jointly invert different geophysical datasets to the end of enforcing the structural similarity of the different physical properties. Fregoso and Gallardo [13] were the first to develop a cross-gradient joint inversion of magnetic and gravity data. Later, Um et al. [14] introduced a coupled inversion of large-scale seismic and electromagnetic data for subsalt imaging. It can be seen as a sequential approach including the cross-gradient constraint term. They split the joint inversion into separate EM, seismic, and cross-gradient inversions. This latter allows to constrain the resistivity model based on a reference velocity model. The resulting resistivity model will serve as an initial model for a new EM separate inversion in an EM refinement process. The approach aimed at an easy minimization of the cross-gradient term. However, the cross-gradient minimization could worsen the data fitting. In the subsequent iteration, the data misfit will be minimized in separate inversions, which could indeed produce a lower structural similarity. Gao and Zhang [15] proposed a strategy to avoid this behavior using the model perturbations resulting from stand-alone inversions to constrain the cross-gradient minimization at each iteration.

Gross [16] introduced an algorithm for a weighted joint inversion of gravity and magnetic data using a cross-gradient constraint. He achieved an improved structural similarity of the models thanks to a local weighting of the cross-gradient. Zhang and Wang [17] introduced a joint inversion based on structural coupling. They adopted a fast gradient algorithm to solve the objective function, which was composed of three terms: the data misfit, the cross-gradient, and the total-variation regularization constraint. This latter led to a more focused and sharp solution. Tavakoli et al. [18] introduced a sequential workflow for the joint inversion of gravity and magnetic data and obtained a successful modeling of evaporite structures. Fang et al. [19] extended the sequential approach to a 3-D joint inversion of gravity and magnetic data. Meng et al. [20], Vatankhah et al. [21], and Zhang et al. [22] proposed different approaches to perform a cross-gradient joint inversion of gravity and magnetic data. Joint inversion of gravity and gravity gradients with cross-gradients were tested on simple synthetic sources for environmental applications [23] and for satellite data in spherical coordinates [24]. Wang et al. [24] obtained improved results with synthetic models of adjacent sources similar to lunar gravity data.

Thanks to the lessons from these works, we adopt a sequential procedure to jointly invert $G_z$ and one of its higher-order vertical derivatives. Note that this is different from previous works on sequential inversion, as we are now searching for the same physical property (density contrasts). We aim to exploit the different wavelength content of $G_z$ and its higher-order vertical derivatives in order to retrieve different and complementary information on both surface and deep sources. We also introduce different types of constraints, either hard or soft. Hard constraints are the reference model and, where available, boundaries on the physical properties from seismic interpretation. Soft constraints are mainly built by introducing the inhomogeneous version of the model weighting function [25]. We seek a compact solution [26], as we aim to recover geological bodies instead of surfaces that would require smoother solutions.

We demonstrate the effectiveness of this strategy, by applying it to a simple synthetic model and to the SEg Advanced Modeling (SEAM) Phase I model. Then, we perform our joint inversion on a real case from Southern Spain, to investigate layered karst systems.

## II. Methodology

### A. Joint Inversion Algorithm

Gallardo and Meju [12] defined the cross-gradient constraint between two physical properties at a given point $(x, y, z)$ with positive $z$-axis pointing downward as follows:

$$\boldsymbol{\tau}(\rho, q) = \nabla\rho(x, y, z) \times \nabla q(x, y, z) \tag{1}$$

where $\rho$ and $q$ are two physical properties. In a 2-D case, we have only the $\tau_y$ of the cross-gradient as the $x$- and $z$-components vanish.

We add the cross-gradient constraint as a penalty term to the objective function [27]. In this case, the combined objective function for the joint inversion of two datasets is

$$\psi(\rho, q) = \varphi_1(\rho) + \varphi_2(q) + \chi(\rho, q) \tag{2}$$

where $\varphi_1(\rho)$ and $\varphi_2(q)$ contains the data-misfit and the model-norm terms for each dataset; $\chi(\rho, q)$ is the norm of the cross-gradient; subscripts 1 and 2 refer, respectively, to the two different datasets; and $\rho$ and $q$ are the two different physical parameter vectors.

Following the purpose of this work, we now rewrite (1) as follows:

$$\boldsymbol{\tau}(\rho_1, \rho_2) = \nabla\rho_1(x, y, z) \times \nabla\rho_2(x, y, z) \tag{3}$$

where $\rho_1$ and $\rho_2$ refer to density models recovered from the gravity and the gravity gradient, respectively.

Equation (2) becomes

$$\psi(\rho_1, \rho_2) = \varphi_1(\rho_1) + \varphi_2(\rho_2) + \chi(\rho_1, \rho_2) \tag{4}$$

where $\varphi_1(\rho_1)$ and $\varphi_2(\rho_2)$ are the gravity and gravity gradient data objective functions and $\chi(\rho_1, \rho_2)$ is the 2-D cross-gradient.

At each $j$th iteration, the model perturbations $\Delta\boldsymbol{\rho}_{1j}$ and $\Delta\boldsymbol{\rho}_{2j}$ are determined via separate inversions and used to constrain the cross-gradient term minimization. The system for the joint inversion of two datasets through the minimization of the cross-gradient term $\chi(\rho_1, \rho_2)$ is after [15]

$$\begin{bmatrix} \mathbf{I} & 0 \\ 0 & \mathbf{I} \\ \mathbf{t_1} & \mathbf{t_2} \end{bmatrix} \begin{bmatrix} \Delta\hat{\boldsymbol{\rho}}_{1j} \\ \Delta\hat{\boldsymbol{\rho}}_{2j} \end{bmatrix} = \begin{bmatrix} \Delta\boldsymbol{\rho}_{1j} \\ \Delta\boldsymbol{\rho}_{2j} \\ -\boldsymbol{\tau} \end{bmatrix} \tag{5}$$

where $\mathbf{I}$ is the identity matrix; $\mathbf{t}_1$ and $\mathbf{t}_2$ are the partial derivative matrices ($\partial\tau/\partial\rho_1$ and $\partial\tau/\partial\rho_2$, respectively) of the 2-D cross-gradient. The solutions of (5) are the cross-gradient constrained model perturbations $\Delta\hat{\boldsymbol{\rho}}_{1j}$ and $\Delta\hat{\boldsymbol{\rho}}_{2j}$. In this way, we constrain the cross-gradient minimization with the model perturbations retrieved from separate inversions. Tavakoli et al. [18] used this strategy as the key step for their sequential joint inversion algorithm.

### B. Separate Inversions

The statement of any inverse problem is the relationship between model parameters and data. If $N$ samples have been measured in an experiment, we can represent them as the data vector $\mathbf{d}$ of length $N$. In the same way, model parameters are represented as the elements of the vector $\mathbf{m}$ of length $M$. Both the gravity and its $h$th derivative forward problems arise in the linear form

$$\mathbf{d} = \mathbf{A}\mathbf{m} \tag{6}$$

where the matrix $\mathbf{A}$ is referred to as the kernel and is sized $N \times M$.

The most common formulation of the inverse problem is that based on the Tikhonov et al. [28] regularization. The idea is to retrieve a regularized solution $\mathbf{m}_\mu$ as the minimum of the combination of a residual norm and the side constraint [29]

$$\min\left\{\|(\mathbf{A}\mathbf{m}-\mathbf{d})\|_2^2 + \mu^2\|\mathbf{L}\mathbf{m}\|_2^2\right\} \tag{7}$$

where $\|\mathbf{A}\mathbf{m}-\mathbf{d}\|_2$ is the $L_2$ norm misfit between the values $\mathbf{A}\mathbf{m}$ and the observed data $\mathbf{d}$, measuring how the retrieved model fits observed data; $\|\mathbf{m}\|_2^2$ is the side constraint, measuring the properties of the model; and $\mathbf{L}$ is the model-weighting matrix and $\mu$ is the regularization parameter, which weighs the minimization of the side constraint with respect to that of the residual norm. For the sake of simplicity, we assume that data errors in (7) are uncorrelated and of the same variance. So, we can omit the data weighting matrix, usually expressed by the covariance matrix $\mathbf{C}^{-1}$ [30]. $\mathbf{L}$ could include several types of a priori information on the model (i.e.: depth weighting function, compactness, reference model, etc.).

In fact, in ambiguous problems, like the potential field one, the density model strictly relates to the supplied a priori information. For example, the minimum-length assumption is the simplest solution for underdetermined inversion problems. However, this type of formulation implies a priori information in the form that the solution is the shortest, it is to say that it must be shallow and characterized by low values of the physical property.

Requiring compactness for the sources is another form of a priori information, which is indeed a strong requirement [10]. In this framework, different authors proposed to adopt a compactness constraint [26], [31], [32] based on the minimization of the area or the volume. In the 2-D case, Last and Kubik [26] assumed a discretization of the source section in $M$ cells and proposed the following definition of area:

$$\text{area} = \text{sp}\lim_{\varepsilon\to 0}\sum_{k=1}^{M}\frac{m_k^2}{m_k^2+\varepsilon^2} \tag{8}$$

where $\varepsilon$ is a small positive number needed to avoid the singularity when $m_k = 0$; $s$ and $p$ are the dimensions of each $k$th cell.

This leads to a model weighting function in the form of the following equations:

$$L_k = \left(m_k^2 + \varepsilon\right)^{-1}. \tag{9}$$

Thus, by introducing (9) in (7), we obtain

$$\mathbf{m} = \arg\min_{\mathbf{m}}\left\{\|\mathbf{A}\mathbf{m}-\mathbf{d}\|_2^2 + \mu^2\sum_{k=1}^{M}\frac{m_k^2}{m_k^2+\varepsilon^2}\right\}. \tag{10}$$

However, further requirements may be accounted for by choosing a specific model weighting function. Portniaguine and Zhdanov [32] proposed to insert a model weighting function in the form of the square root of the sensitivity matrix. This approach led to a diagonal matrix, meaning that a constant weight is attributed to each layer in which the model is subdivided [33]. For this reason, deeper levels are weighted more than shallower ones as the function scales the model parameters with the sensitivity of kernel $\mathbf{A}$.

We note that this form of a priori information is close to the one suggested by Li and Oldenburg [34], [35], with the weighting function expressed as follows:

$$w(x, y, z) = \frac{1}{z^\beta} \tag{11}$$

where $z$ is the depth of each layer in the model and $\beta$ is an exponent depending on the type of potential field: $\beta = 2$ for gravity data and $\beta = 3$ for magnetic data. The authors proposed these values by analyzing the decay of the field of a single cell, in which the source volume is subdivided. However, the field decay of a single cell has nothing to do with the source distribution, which is the only quantity that determines the decay of the field. For example, the decay of the field of a sphere is different from that of a fault, independently of the way (e.g., number of blocks, types of blocks) the source volume is parametrized.

To fix this issue, Cella and Fedi [36] introduced a model depth weighting exponent $\beta$ with a physics-related value, which effectively depends on the model. They started from the homogeneity law [37], [38] and demonstrated that an appropriate value of $\beta$ is $\beta = N$, where $N$ is the structural index of the source, rather than the power-law decay of a single cubic cell. $N$ may be estimated by specific techniques [39], [40], [41], [42], [43], [44], [45], [46] or it may be assumed as a priori information on the type of source. In this sense, note that previous formulation [34], [35] becomes a particular case of this more general relationship, since $\beta = N = 3$ holds only for homogeneous, spherical-like, source distributions. The good behavior of this approach in compact inversions has been discussed and the role of an appropriate model weighting function has been proved to be even more important in joint inversions [47], [48]. More recently, Vitale and Fedi [25] generalized the approach of Cella and Fedi [36], for fields generated by complex source distributions. They proposed to assign $\beta$ at every block of the source-domain and

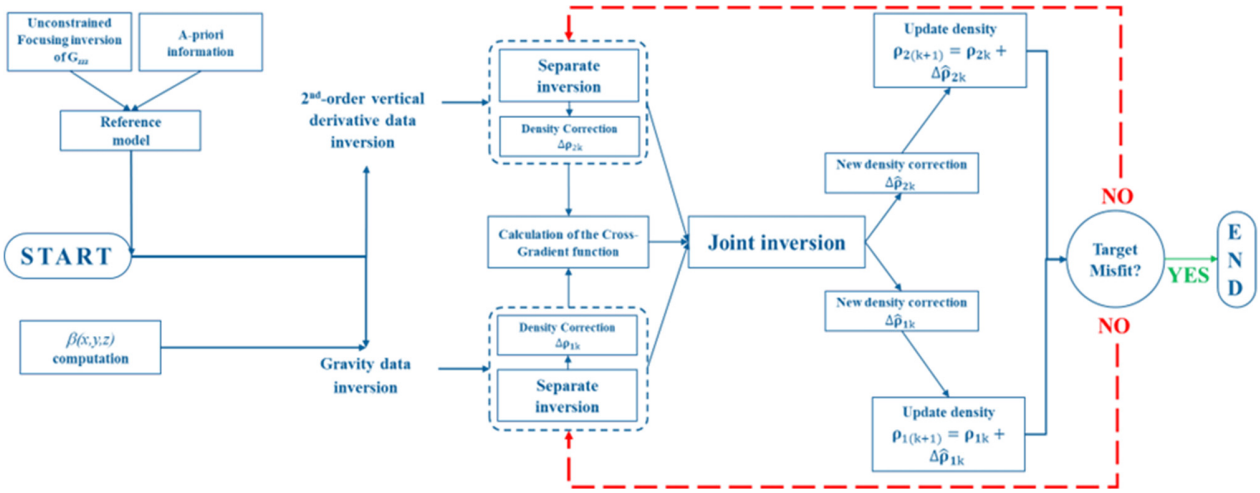


Fig. 1. Workflow.

defined the model depth weighting function as follows:

$$w(x, y, z) = \frac{1}{z^{\left[\frac{\beta(x,y,z)}{2}\right]}} \tag{12}$$

where $\beta(x, y, z)$ is the depth weighting exponent in the source-domain. We highlight that the inhomogeneous approach brings a different weight for each $k$th cell of the model instead of a constant value for each layer. Equation (12) is based on the work by Fedi et al. [42], who stated that in the harmonic region, any real field could be well approximated by a homogenous field in a local sense. This leads to generalizing the homogeneity equation into a multihomogeneity law, with any real fields being characterized by a fractional and spatially inhomogeneous homogeneity degree. To compute $\beta(x, y, z)$ for potential fields, it is necessary to estimate the homogeneity degree $n(x, y, -z)$ of the field at different scales or altitudes. This brings to the necessity to upward continue the measured field. In order to estimate $n$, we evaluate the scaling function of the field at many altitudes [43], [46]. $\beta(x, y, z)$ is so evaluated as follows:

$$\beta(x, y, z) = N(x, y, z) = -n(x, y, -z) + h \tag{13}$$

where $h$ indicates the differentiation order of the magnetic field or of the gravity gradient and the change of sign of $z$ indicates that every value of $n$ estimated in the harmonic region is attributed to the specular position in the source-region.

In conclusion, we may define the model weighting function for the $k$th block as follows:

$$L_k = w_k\left(m_k^2 + \varepsilon\right)^{-1}. \tag{14}$$

So, (7) becomes

$$\mathbf{m} = \arg\min_{\mathbf{m}}\left\{\|\mathbf{Am} - \mathbf{d}\|_2^2 + \mu^2 \sum_{k=1}^{M} \frac{w_k^2 m_k^2}{m_k^2 + \varepsilon^2}\right\}. \tag{15}$$

Finally, our algorithm can incorporate a reference model ($m_{\text{ref}}$) as follows:

$$\mathbf{m} = \arg\min_{\mathbf{m}}\left\{\|\mathbf{Am} - \mathbf{d}\|_2^2 + \mu^2 \sum_{k=1}^{M} \frac{w_k^2 (m - m_{\text{ref}})_k^2}{(m - m_{\text{ref}})_k^2 + \varepsilon^2}\right\}. \tag{16}$$

### C. Joint Inversion Workflow

Unless simple cases involve a single source, potential field anomalies are produced by the superposition of different source contributions, which interfere with each other. Thus, many methods address the inversion problem by first separating the effects of sources seated at different depths, but this is one of the trickiest tasks in potential field modeling. In general, standard filters often do not accomplish satisfactorily this task, mainly because they are merely mathematical tools applied to physical signals. Instead, physically based transformations, such as upward continuation or differentiation may be more useful. In our joint inversion, we try to take advantage from gravity and its $h$th-order vertical derivatives, because they enhance different contents at medium-to-large wavelengths and at medium-to-short wavelengths, respectively. We now define our workflow (see Fig. 1) for vertically stacked sources modeling of $G_z$ and its second-order derivative $G_{zzz}$. Other combinations may be exploited that could involve also fractional-order derivatives [49]. Prior to jointly invert our data, we proceed with the computation of the inhomogeneous depth weighting function (12). We compute $\beta(x, y, z)$ on $G_z$ because it has a most complete set of contributions from deep to shallow sources. In addition, we can build a reference model by finding an unconstrained compact solution for $G_{zzz}$. It is to say we impose $\beta = 0$. Letting the compactness to guide the process, we obtain a preliminary model of the shallow sources with only slight contributions from the deep-seated ones. We can enhance this reference model with hard constraints from interpretation of other geophysical data or geological/direct knowledge of the area (i.e.: wells, field geology, etc.). The computation of high-order derivatives could result in a rather low signal-to-noise. However, sometimes, the first-order vertical derivative $G_{zz}$ is directly measured, especially during GGT surveys. These measurements could be very useful to obtain stable higher-order derivatives. Usually, vertical derivatives of potential fields may be computed numerically; here, we adopt the stable algorithm of the integrated second vertical derivative (ISVD) procedure [50]. Once we have formed the two datasets, we must define the a priori

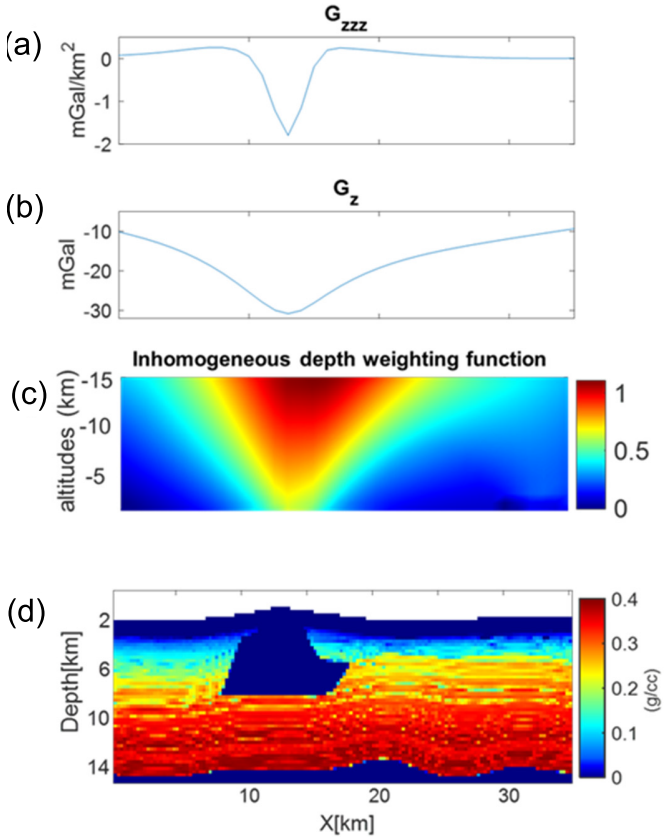


Fig. 2. (a) $G_{zzz}$. (b) $G_z$. (c) $\beta(x, y, z)$. (d) Synthetic density model.

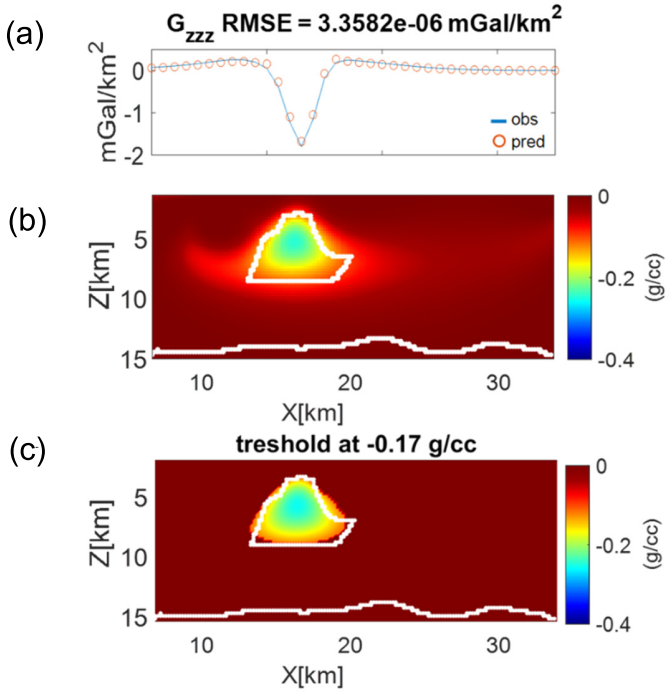


Fig. 3. (a) Observed and predicted data. (b) $G_{zzz}$ inversion with $\beta(x, y, z) = 0$. (c) Model in a with an imposed threshold of $-0.17$ g/cc.

information that we want to express in the model weighting matrix $\mathbf{L}$ as specified before and then move to the joint inversion.

The workflow exploits the powerfulness of a joint inversion thanks to decoupling the minimization of the combined objective function in (4), in which the cross-gradient minimization is used as a constraint on the iterative updates of the model perturbations as in (5). Thus, we can expect that the cross-gradient minimization could help to balance the gravity field inversion, which regards deep and shallow source contributions, with that of the second-order vertical derivative of gravity, which would include especially the contributions related to the shallowest sources. We want to stress this aspect, as it represents a new point of view on the joint inversion of potential fields. Special tools will be used to make an adequate diagnostic of the validity of the model and of the joint inversion (see synthetic tests and real case sections).

## III. Synthetic Modeling

### A. SEAM-Phase I Model

To test our approach with a synthetic realistic model, we chose the SEAM- Phase I model [51]. It is a 3-D synthetic model based on a deep-water salt domain in the Gulf of Mexico. It includes a complex salt intrusive and its mother-salt in a folded Tertiary basin. The physical properties of the model and the related geophysical simulations are designed to provide key tools for testing algorithms and workflow in a realistic scenario. In fact, the model includes common challenges faced in geophysical exploration, while having a defined target to compare obtained results. We illustrate the result obtained on the 2-D profile extracted at $y = 4000$ m [Fig. 2(d)]. The model consists of $135 \times 60$ cubic cells with side size of 250 m for a total length of 34 km and a 15 km maximum depth. The salt dome extends from 3 to about 8 km, while the top autochthonous salt layer is deeper than 12 km. Together with $G_z$ [Fig. 2(b)], we compute $G_{zzz}$ [Fig, 2(a)] and the inhomogeneous depth weighting function on $G_z$ [Fig. 2(c)]. In [Fig. 3(b)], we show the result of a compact inversion of $G_{zzz}$ under the assumption of a homogeneous $\beta$ equal to 0. It is clear that we are modeling in a reasonable way only the shallowest source. The contribution of the deep-seated source is not forced to the deeper portions of the model, but it is modeled as a diffuse source around the salt dome. Its density-contrast is very low, which is geologically unreliable. In Fig. 3(a), we can appreciate the low data misfit given by the root mean square error (RMSE). However, applying a threshold of $-0.17$ g/cc to the model, we may isolate better the contribution of the salt dome [Fig. 3(c)] and use it as reference model in the joint inversion. The results of the joint inversion are shown in Fig. 5. We begin to describe the models resulting from separate inversions. They are clearly not able to produce an adequate modeling of the salt features. $G_z$ inversion [Fig. 4(a)] produces a model that correctly recover an increasing density contrast with depth but joins the salt dome to the mother salt. This behavior is lost in the inversion of $G_{zzz}$ [Fig. 4(b)], which produces a compact salt dome but with a deep root connecting it to the mother salt. Nevertheless, both models even if they have a low data misfit, they could not fix the vertical separation of the salt dome from its mother salt, which is significant in basin modeling. On the

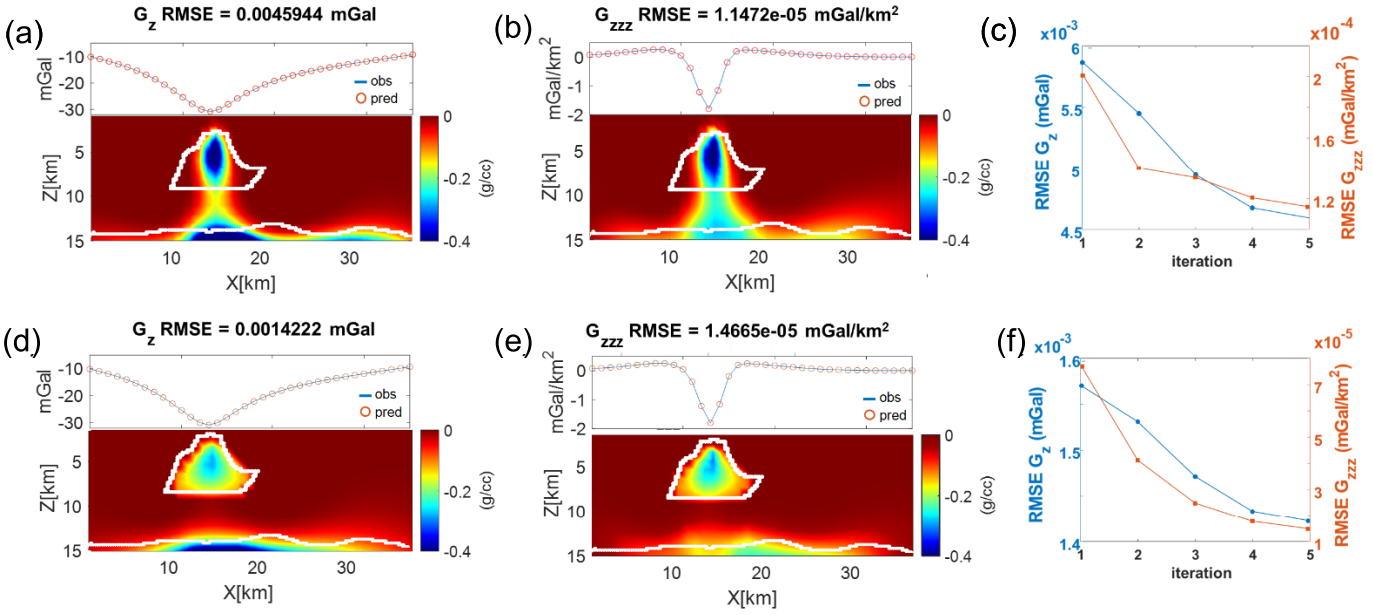


Fig. 4. Model resulting from (a) separate inversion of $G_z$. (b) Separate inversion of $G_{zzz}$. (c) Convergence plots for separate inversions. (d) MOSJI on $G_z$. (e) MOSJI on of $G_{zzz}$. (f) convergence plots for joint inversion.

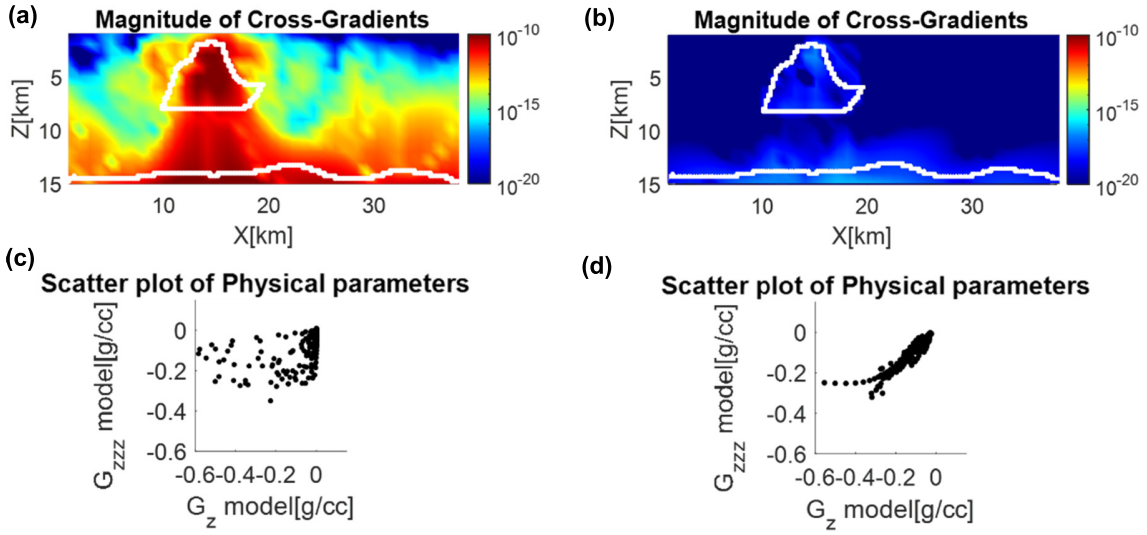


Fig. 5. (a) Cross-gradients value of separate inversions. (b) Scatter plot of density models of separate inversions. (c) Magnitude of cross-gradient value of MOSJI joint inversion. (d) Scatter plot of density models of MOSJI joint inversion.

other hand, in the joint inversion, $G_z$ [Fig. 4(d)] is more able to retrieve a rather complete model of the investigated subsurface volume while we can see that $G_{zzz}$ [Fig. 4euro] produces a model with only the shallower source modeled in a proper way, while targeting comparable values of data misfit to those of separate inversions. The convergence plots of joint inversion [Fig. 4(f)] are comparable to those of the separate inversions. These plots demonstrate a similar computation efficiency while including more constraints which lead to more reliable solutions. As obvious, one of the improvements is the enhanced structural similarity in the joint inversion models. In fact, looking at the magnitude of cross-gradient values of the separately inverted models, jointly inverted models [Fig. 5(a) and (b)], we can appreciate a strong decrease in the absolute values. It is also useful to compare the arrangement of these values. While the separate inversions show values which distribute on the whole space from the position of the shallow-seated source toward depth, in the joint inversion models, they are concentrated at the boundaries of the shallower source, meaning that only details due the discretization of the model-space can be reviewed. An insightful result is obtained when looking at the scatter plots of the recovered physical parameters. We can appreciate the linearization of the values in the jointly inverted models [Fig. 5(d)] with respect to common separate inversions [Fig. 5(c)]. We can describe a diagonal linear cluster. This diagonal trend has a differentiated behavior in its final portion. In fact, some values with lower values in the $G_z$ model assume a higher value in $G_{zzz}$. This is because the

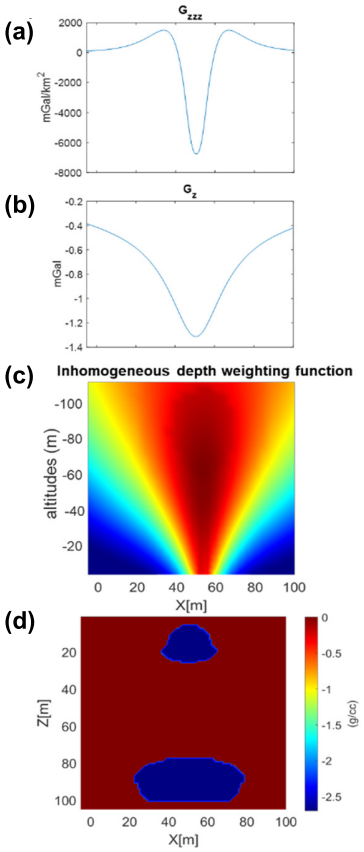


Fig. 6. (a) $G_{zzz}$. (b) $G_z$. (c) $\beta(x, y, z)$. (d) Synthetic density model.

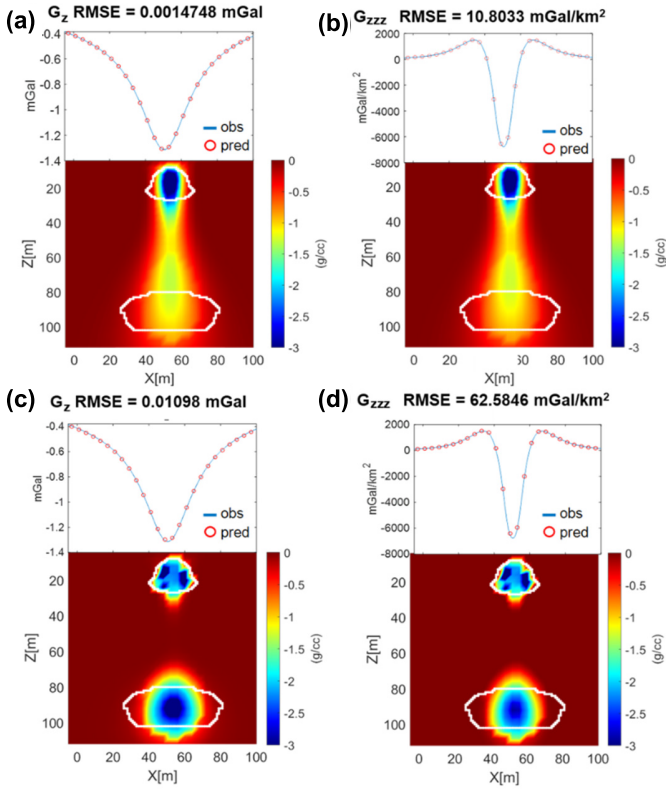


Fig. 7. Model resulting. (a) Separate inversion of $G_z$. (b) Separate inversion of $G_{zzz}$. (c) MOSJI on $G_z$. (d) MOSJI on of $G_{zzz}$.

sensitivity of $G_{zzz}$ is addressed toward the salt dome, which cause less accuracy in modeling the mother salt. It is important

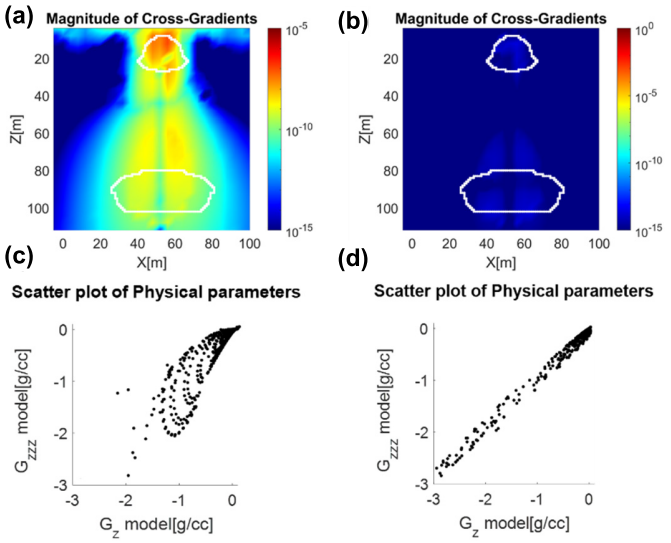


Fig. 8. (a) Magnitude of cross-gradient value of separate inversions. (b) Scatter plot of density models of separate inversions. (c) Magnitude of cross-gradients value of MOSJI. (d) Scatter plot of density models of MOSJI.

to note that the salt dome has an average density contrast of −0.2 g/cc. For layered models, this is justified as the retrieved density distribution takes the meaning of an equivalent density contrast. It is to say that we have an actual density contrast varying with depth, but we recover from inversion a value close to the weighted mean. This concept was introduced to describe an equivalence between a stratified basin and a basin having the same shape but filled homogeneously with an average density [52]. The same equivalence was demonstrated in salt dome modeling with different density contrasts at the various layers [46].

### B. Karst Model

The karst model [Fig. 6(d)] is a grid of 50 × 50 cells sized 2 × 2 m. It contains two bodies at different depths. This setting represents a very complex but common challenge in karst cavities detection for hazard assessment. The density contrast between the sources and the background is set at −2.7 g/cc. The synthetic $G_z$ [Fig. 6(b)] was computed with spacing of 2 m, while $G_{zzz}$ [Fig. 6(a)] was obtained thanks to the ISVD method. Following the procedure described in Section II, we computed $\beta(x, y, z)$ matrix based on the $G_z$ data Fig. 6(c). Separate inversions do not produce a clear separation between the two sources. In the model retrieved from $G_{zzz}$ inversion [Fig. 7(b)], the deep-seated source appears as a low-density diffuse source. At the same time, the density of the shallowest source is clearly overestimated. Model resulting from $G_z$ [Fig. 7(a)], produce a similar model, still missing a proper density contrast, lateral extension, and depth position. We can note that in this latter model, we have a slightly improved recover of the deep-seated cavity. This reflects the fact that $G_z$ brings more information on the deepest source. In general, we can state that nor the $G_z$ or $G_{zzz}$ are able to recover a correct density distribution with only separate inversions.

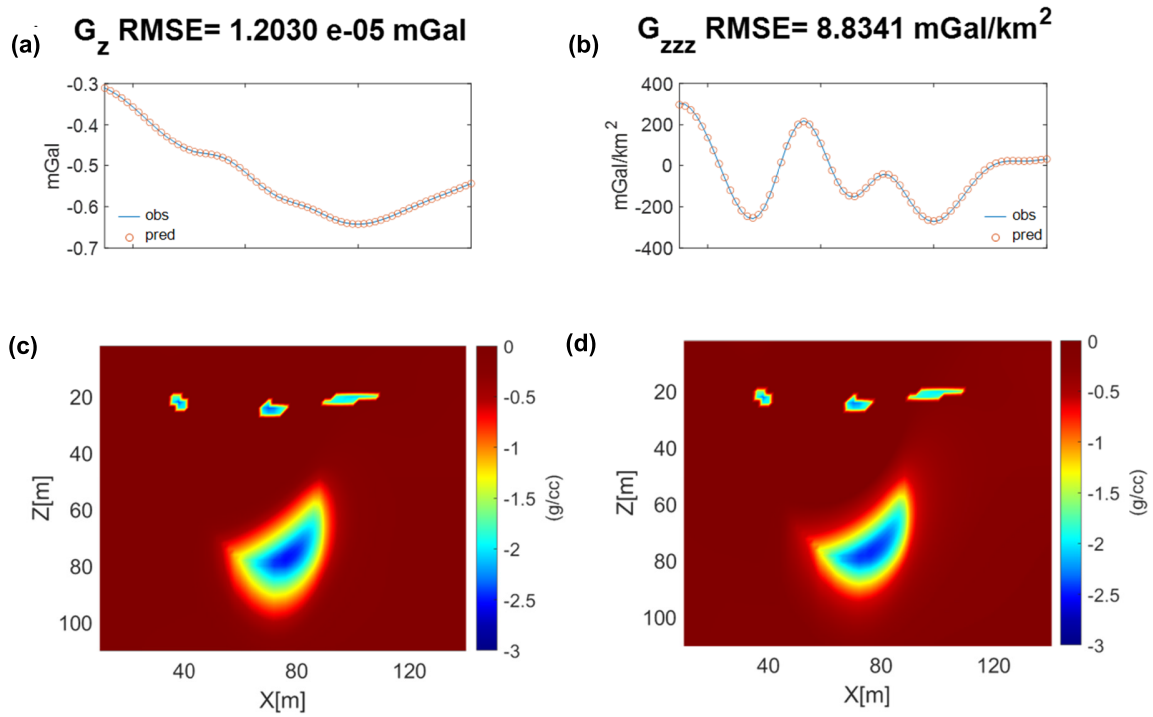


Fig. 9. (a) Observed and predicted $G_z$. (b) Observed and predicted $G_{zzz}$. (c) Model resulting from joint inversion of $G_z$. (d) Model resulting from joint inversion of $G_{zzz}$.

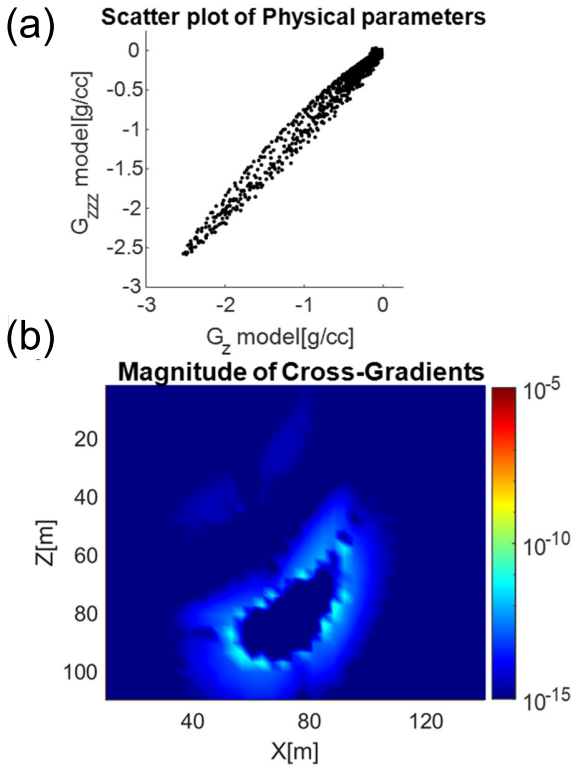


Fig. 10. (a) Scatter plot of physical parameters. (b) Magnitude of cross-gradient values.

We now adopt the described workflow for the multiorder sequential joint inversion (MOSJI). So, we used the described procedure to build a reference model and the inhomogeneous model weighting function for $G_z$. Both the $G_z$ and $G_{zzz}$ models [Fig. 7(c) and (d)] are instead able to describe the shallower and the deep-seated sources. We can see a rather accurate positioning of the cavities with a proper density contrast. The model resulting from $G_z$ [Fig. 7(c)] recovers slightly better the deeper source with an improved overall positioning and extension of the cavity when compared to that produced by $G_{zzz}$. Once again, this reflects the different sensitivities brought by the dataset. We noticed that the same considerations done before for the data misfit are valid also in this case.

The analysis of the cross-gradient values [Fig. 8(a) and (b)] confirms the results obtained in the synthetic test at a basin scale. The most interesting result is that in this case, we obtain a linearization of the physical parameters in the cross-plot of the jointly inverted models [Fig. 8(d)] with respect to that of separate inversions [Fig. 8(c)]. In this case, we can appreciate that we lose the divergent behavior in the tail of the cluster observed in the previous test [Fig. 5(d)]. This is due to the fact that in this model, both the sources have the same density contrast.

## IV. Real Case

We now apply our method to a real case for cavity detection in Southern Spain. We investigated the Gruta de las Maravillas in Aracena. It was previously studied by Martínez-Moreno et al. [53] and interpreted with forward modeling. The cave lies within marbles and its genesis is due to the dissolution of these rocks. It consists of three different levels with a water table that is present at 650 m a.s.l [54]. We performed our joint inversion on the central part of the Line 4 [53], that we resampled at 2 m [Fig. 9(a)]. We computed the $G_{zzz}$ [Fig. 9(b)]

as already discussed. Further information on the gravity data can be found on the aforementioned works. The zero-level of our model coincides with the maximum of the topography of the line. Our model consists of 50 × 35 cubic cells with a side dimension of 2 m. In this case, we used a reference model with the solution of an unconstrained preliminary inversion of $G_{zzz}$, which was cut at a threshold of −2.5 g/cc. This is justified as a known density contrast of void in marbles.

Results suggest the presence of three shallow cavities with a density contrast of around 2.7 g/cc, which well represents a typical density contrast of air-filled cavities within marbles [Fig. 9(c) and (d)]. These three sources have been also retrieved in the modeling of Martìnez-Moreno et al. [53]. The horizontal position is consistent between the forward model and our interpretation, locating the shallow-seated group of cavities at a distance from 180 to 250 m on the original line. The central cavity of the group is slightly deeper in our modeling than in the forward model [53], which locates this cavity at about 20 m depth.

Following our approach, once again we are able to model the deepest sources [Fig. 9(c) and (d)], thanks to their different wavelength-content. We found a deeper cavity with its center at about 80 m depth and with a 50 m extension. The forward modeling performed [53] proposed an elongated horizontal source between 50- and 75-m depth. The positioning is slightly different in the two interpretations, but their ranges are comparable. In addition, forward model [53] suggested an elongated appendix on the upper right corner of this cavity. We have a confirmation of this possible features in our modeling. Martìnez-Moreno et al. [53] provide also resistivity, induced polarization, and seismic modeling on the same profile. Seismic data modeling clearly shows the presence of the two lateral sallower cavities as low velocity zones with a low number of rays respectively in the velocity model and ray tracing coverage model. The central cavity is not clearly interpretable, but its presence is confirmed by gravity modeling presented both here and in the aforementioned work [53]. Resistivity and Induced Polarization model are more informative on the elongated appendix of the deeper sources which is recovered in our results and suggested by the forward modeling [53]. Analysis of the cross-gradient [Fig. 10(a)] is comparable in magnitude and distribution with those obtained in synthetic tests, with the highest values located on the edges of sources. In the end, we obtain a linearization in the cross-plot of physical parameters [Fig. 10(b)].

## V. Conclusion

We propose a new approach to joint inversion of gravity data for vertically stacked source modeling. It is based on the sequential strategy introduced by Tavakoli et al. [18] but it is here applied to recover the same physical property (density) from two different quantities: gravity field and its second-order vertical derivative. To achieve our aim, we built an algorithm for compact inversion which can incorporate several types of constraints.

In particular, we adopted the inhomogeneous model weighting function [25] and a reference model in which we can introduce the available a priori information. Thanks to this approach, we interpreted both shallow and deep-seated sources. This is possible because we used a workflow designed to exploit the different wavelength-content between vertical derivatives of different order. Results on both simple synthetic, realistic synthetic, and real case demonstrated the ability to recover reliable density distributions. When compared to results of common separate inversion, our algorithm improved our ability to perform vertically stacked source modeling, which is one of the trickiest tasks in applied geophysics. An interesting analysis of the joint inversion results is yielded by the cross-gradient values demonstrating an improved structural similarity. This is also better substantiated in the cross-plot of physical parameters, which show a meaningful linearization and clusterization of the retrieved parameters.

These results open a new point of view on the joint inversion of gravity and gravity vertical gradients. In fact, we have found that to fully exploit the different information of each dataset, decoupled minimization of the objective function could be more useful than minimizing the whole function, as commonly done. In this way, we retrieve different models with different information and address the joint model toward a complete description of the sources, either shallow or deep. We applied our method on different scale scenarios (from near-surface microgravity to basin-scale) and proved it to be effective in all of them. Obviously, this approach could be applied to joint inversion of different orders of vertical derivation of magnetic anomalies as well. In addition, the concept we are proposing is easily transportable from 2-D to 3-D Earth models, which will be the most immediate step of our work.

## References


[1] H. Cavendish, "XXI. Experiments to determine the density of the earth," *Phil. Trans. Roy. Soc. London*, vol. 88, pp. 469–526, Dec. 1798, doi: 10.1098/rstl.1798.0022.

[2] R. V. Eötvös, "Untersuchungen über gravitation und erdmagnetismus," *Annalen der Physik*, vol. 295, no. 10, pp. 354–400, Jan. 1896.

[3] R. E. Bell, "Gravity gradiometry," *Sci. Amer.*, vol. 278, no. 6, pp. 74–79, 1998. [Online]. Available: http://www.jstor.org/stable/26057859.

[4] Y. Li, "3-D inversion of gravity gradiometer data," in *Proc. SEG Tech. Program Expanded Abstr.*, 2001, pp. 1470–1473.

[5] M. S. Zhdanov, R. Ellis, and S. Mukherjee, "Three-dimensional regularized focusing inversion of gravity gradient tensor component data," *Geophysics*, vol. 69, no. 4, pp. 925–937, Jul. 2004, doi: 10.1190/1.1778236.

[6] C. Martinez and Y. Li, "Inversion of regional gravity gradient data over the vredefort impact structure, south Africa," in *Proc. SEG Tech. Program Expanded Abstr.*, Jan. 2011, pp. 841–845.

[7] E. K. Biegert, M. Talwani, and D. J. Smit, "Gravity gradients for de-risking prestack depth migration," in *Proc. 63rd EAGE Conf. Exhib.*, 2001, Paper cp-15, doi: 10.3997/2214-4609-pdb.15.IG-2.

[8] J. Capriotti and Y. Li, "Gravity and gravity gradient data: Understanding their information content through joint inversions," in *Proc. SEG Tech. Program Expanded Abstr.*, Aug. 2014, pp. 1329–1333.

[9] V. Paoletti, M. Fedi, F. Italiano, G. Florio, and S. Ialongo, "Inversion of gravity gradient tensor data: Does it provide better resolution?" *Geophys. J. Int.*, vol. 205, no. 1, pp. 192–202, Feb. 2016, doi: 10.1093/gji/ggw003.

[10] S. Ialongo, M. Fedi, and G. Florio, "Invariant models in the inversion of gravity and magnetic fields and their derivatives," *J. Appl. Geophys.*, vol. 110, pp. 51–62, Nov. 2014.

[11] J. Capriotti and Y. Li, "Joint inversion of gravity and gravity gradient data: A systematic evaluation," *Geophysics*, vol. 87, no. 2, pp. 29–44, Mar. 2022, doi: 10.1190/geo2020-0729.1.

[12] L. A. Gallardo and M. A. Meju, "Characterization of heterogeneous near-surface materials by joint 2D inversion of DC resistivity and seismic data," *Geophys. Res. Lett.*, vol. 30, no. 13, p. 1658, Jul. 2003, doi: 10.1029/2003GL017370.

[13] E. Fregoso and L. A. Gallardo, "Cross-gradients joint 3D inversion with applications to gravity and magnetic data," *Geophysics*, vol. 74, no. 4, pp. 31–42, Jul. 2009, doi: 10.1190/1.3119263.

[14] E. S. Um, M. Commer, and G. A. Newman, "A strategy for coupled 3D imaging of large-scale seismic and electromagnetic data sets: Application to subsalt imaging," *Geophysics*, vol. 79, no. 3, pp. 1–13, May 2014, doi: 10.1190/geo2013-0053.1.

[15] J. Gao and H. Zhang, "An efficient sequential strategy for realizing cross-gradient joint inversion: Method and its application to 2-D cross borehole seismic traveltime and DC resistivity tomography," *Geophys. J. Int.*, vol. 213, no. 2, pp. 1044–1055, May 2018, doi: 10.1093/gji/ggy026.

[16] L. Gross, "Weighted cross-gradient function for joint inversion with the application to regional 3-D gravity and magnetic anomalies," *Geophys. J. Int.*, vol. 217, no. 3, pp. 2035–2046, Jun. 2019, doi: 10.1093/gji/ggz134.

[17] Y. Z. A. Y. W. Sci, "Three-dimensional gravity-magnetic cross-gradient joint inversion based on structural coupling and a fast gradient method," *J. Comput. Math.*, vol. 37, no. 6, pp. 758–777, Jun. 2019.

[18] M. Tavakoli, A. N. Kalateh, M. Rezaie, L. Gross, and M. Fedi, "Sequential joint inversion of gravity and magnetic data via the cross-gradient constraint," *Geophys. Prospecting*, vol. 69, no. 7, pp. 1542–1559, Sep. 2021, doi: 10.1111/1365-2478.13120.

[19] Y. Fang, J. Wang, X. Meng, S. Zheng, and H. Tang, "An efficient cross-gradient joint inversion algorithm for gravity and magnetic data using a sequential strategy," *IEEE Trans. Geosci. Remote Sens.*, vol. 60, pp. 1–16, 2022, Art. no. 4510116, doi: 10.1109/TGRS.2022.3182690.

[20] Q. Meng, G. Ma, L. Li, T. Wang, and J. Han, "3-D cross-gradient joint inversion method for gravity and magnetic data with unstructured grids based on second-order Taylor formula: Its application to the southern greater Khingan range," *IEEE Trans. Geosci. Remote Sens.*, vol. 60, pp. 1–16, 2022, Art. no. 5914816, doi: 10.1109/TGRS.2022.3172337.

[21] S. Vatankhah, S. Liu, R. A. Renaut, X. Hu, J. D. Hogue, and M. Gharloghi, "An efficient alternating algorithm for the $L_p$-norm cross-gradient joint inversion of gravity and magnetic data using the 2-D fast Fourier transform," *IEEE Trans. Geosci. Remote Sens.*, vol. 60, pp. 1–16, 2022, Art. no. 4500416, doi: 10.1109/TGRS.2020.3033043.

[22] R. Zhang, T. Li, and C. Liu, "Joint inversion of multiphysical parameters based on a combination of cosine dot-gradient and joint total variation constraints," *IEEE Trans. Geosci. Remote Sens.*, vol. 60, pp. 1–10, 2022, Art. no. 5902710, doi: 10.1109/TGRS.2021.3071498.

[23] L. Bianco, M. Tavakoli, A. Vitale, and M. Fedi, "Workflow for a joint inversion of gravity and gravity gradients for environmental applications," in *Proc. 2nd Int. Meeting Appl. Geosci. Energy*, Aug. 2022, pp. 3645–3649.

[24] N. Wang, G. Ma, L. Li, T. Wang, and D. Li, "A density-weighted and cross-gradient constrained joint inversion method of gravity and vertical gravity gradient data in spherical coordinates and its application to lunar data," *IEEE Trans. Geosci. Remote Sens.*, vol. 60, pp. 1–11, 2022, Art. no. 4511211, doi: 10.1109/TGRS.2022.3196052.

[25] A. Vitale and M. Fedi, "Self-constrained inversion of potential fields through a 3D depth weighting," *Geophysics*, vol. 85, no. 6, pp. 143–156, Nov. 2020, doi: 10.1190/geo2019-0812.1.

[26] B. J. Last and K. Kubik, "Compact gravity inversion," *Geophysics*, vol. 48, no. 6, pp. 713–721, Jun. 1983, doi: 10.1190/1.1441501.

[27] L. A. Gallardo and M. A. Meju, "Structure-coupled multiphysics imaging in geophysical sciences," *Rev. Geophys.*, vol. 49, no. 1, p. 3115, Mar. 2011, doi: 10.1029/2010RG000330.

[28] A. N. Tikhonov, V. J. Arsenin, V. I. K. Arsenin, and V. Y. Arsenin, *Solutions of ill-Posed Problems*. Washington, DC, USA: USA, 1977.

[29] P. C. Hansen, *Rank-Deficient and Discrete ill-Posed Problems: Numerical Aspects of Linear Inversion*. Philadelphia, PA, USA: SIAM, 1998.

[30] P. C. Hansen, *Discrete Inverse Problems: Insight and Algorithms*. Philadelphia, PA, USA: SIAM, 2010.

[31] O. Portniaguine and M. S. Zhdanov, "Focusing geophysical inversion images," *Geophysics*, vol. 64, no. 3, pp. 874–887, May 1999, doi: 10.1190/1.1444596.

[32] O. Portniaguine and M. S. Zhdanov, "3-D magnetic inversion with data compression and image focusing," *Geophysics*, vol. 67, no. 5, pp. 1532–1541, Sep. 2002, doi: 10.1190/1.1512749.

[33] M. Pilkington, "3D magnetic data-space inversion with sparseness constraints," *Geophysics*, vol. 74, no. 1, pp. 7–15, Jan. 2009, doi: 10.1190/1.3026538.

[34] Y. Li and D. W. Oldenburg, "3-D inversion of magnetic data," *Geophysics*, vol. 61, no. 2, pp. 394–408, Mar. 1996, doi: 10.1190/1.1443968.

[35] Y. Li and D. W. Oldenburg, "3-D inversion of gravity data," *Geophysics*, vol. 63, no. 1, pp. 109–119, Jan. 1998, doi: 10.1190/1.1444302.

[36] F. Cella and M. Fedi, "Inversion of potential field data using the structural index as weighting function rate decay," *Geophys. Prospecting*, vol. 60, no. 2, pp. 313–336, Mar. 2012, doi: 10.1111/j.1365-2478.2011.00974.x.

[37] P. Stavrev and A. Reid, "Degrees of homogeneity of potential fields and structural indices of Euler deconvolution," *Geophysics*, vol. 72, no. 1, pp. 1–12, Jan. 2007, doi: 10.1190/1.2400010.

[38] M. Fedi, "Scaling laws in geophysics: Application to potential fields of methods based on the laws of self-similarity and homogeneity," in *Fractal Solutions for Understanding Complex Systems in Earth Sciences*, V. P. Dimri, Ed. Cham, Switzerland: Springer, 2016, pp. 1–18.

[39] A. B. Reid, J. M. Allsop, H. Granser, A. J. Millett, and I. W. Somerton, "Magnetic interpretation in three dimensions using Euler deconvolution," *Geophysics*, vol. 55, no. 1, pp. 80–91, Jan. 1990, doi: 10.1190/1.1442774.

[40] M. Fedi, R. Primiceri, T. Quarta, and A. V. Villani, "Joint application of continuous and discrete wavelet transform on gravity data to identify shallow and deep sources," *Geophys. J. Int.*, vol. 156, no. 1, pp. 7–21, Jan. 2004, doi: 10.1111/j.1365-246X.2004.02118.x.

[41] M. Fedi, "DEXP: A fast method to determine the depth and the structural index of potential fields sources," *Geophysics*, vol. 72, no. 1, pp. 1–11, Jan. 2007, doi: 10.1190/1.2399452.

[42] M. Fedi, G. Florio, and V. Paoletti, "MHODE: A local-homogeneity theory for improved source-parameter estimation of potential fields," *Geophys. J. Int.*, vol. 202, no. 2, pp. 887–900, Jun. 2015, doi: 10.1093/gji/ggv185.

[43] M. Fedi and G. Florio, "SCALFUN: 3D analysis of potential field scaling function to determine independently or simultaneously structural index and depth to source," in *Proc. SEG Tech. Program Expanded Abstr.*, Jan. 2006, pp. 963–967.

[44] G. Florio, M. Fedi, and R. Pasteka, "On the application of Euler deconvolution to the analytic signal," *Geophysics*, vol. 71, no. 6, pp. 87–93, Nov. 2006, doi: 10.1190/1.2360204.

[45] F. Cella, M. Fedi, and G. Florio, "Toward a full multiscale approach to interpret potential fields," *Geophys. Prospecting*, vol. 57, no. 4, pp. 543–557, Jul. 2009, doi: 10.1111/j.1365-2478.2009.00808.x.

[46] M. S. Chauhan, M. Fedi, and M. K. Sen, "Gravity inversion by the multi-homogeneity depth estimation method for investigating salt domes and complex sources," *Geophys. Prospecting*, vol. 66, no. 1, pp. 175–191, Mar. 2018, doi: 10.1111/1365-2478.12603.

[47] M. Milano, R. Varfinezhad, H. Bizhani, M. Moghadasi, A. N. Kalateh, and H. Baghzendani, "Joint interpretation of magnetic and gravity data at the Golgohar mine in Iran," *J. Appl. Geophys.*, vol. 195, Dec. 2021, Art. no. 104476, doi: 10.1016/j.jappgeo.2021.104476.

[48] R. Varfinezhad, M. Fedi, and M. Milano, "The role of model weighting functions in the gravity and DC resistivity inversion," *IEEE Trans. Geosci. Remote Sens.*, vol. 60, pp. 1–15, 2022, Art. no. 4507915, doi: 10.1109/TGRS.2022.3149139.

[49] G. Florio, M. Fedi, and F. Cella, "A fractional vertical derivative technique for regional-residual separation," *Geophys. J. Int.*, vol. 232, no. 1, pp. 601–614, Oct. 2022, doi: 10.1093/gji/ggac348.

[50] M. Fedi and G. Florio, "Detection of potential fields source boundaries by enhanced horizontal derivative method," *Geophys. Prospecting*, vol. 49, no. 1, pp. 40–58, Jan. 2001, doi: 10.1046/j.1365-2478.2001.00235.x.

[51] M. Fehler and P. J. Keliher, *SEAM Phase 1: Challenges of Subsalt Imaging in Tertiary Basins, With Emphasis on Deepwater Gulf of Mexico*. Houston, TX, USA: Society of Exploration Geophysicists, 2011.

[52] V. A. Litinsky, "Concept of effective density: Key to gravity depth determinations for sedimentary basins," *Geophysics*, vol. 54, no. 11, pp. 1474–1482, Nov. 1989, doi: 10.1190/1.1442611.

[53] F. J. Martínez-Moreno et al., "Integrated geophysical methods for studying the Karst system of Gruta de las Maravillas (Aracena, Southwest Spain)," *J. Appl. Geophys.*, vol. 107, pp. 149–162, Aug. 2014.

[54] F. J. Martínez-Moreno et al., "The Gruta de las Maravillas (Aracena, South-West Iberia): Setting and origin of a cave in marbles from dissolution of pyrite," *Geomorphology*, vol. 253, pp. 239–250, Jan. 2016.

**Luigi Bianco** received the M.Sc. (Hons.) degree in geology and applied geology from the University of Naples Federico II, Naples, Italy, in 2021, where he is currently pursuing the Ph.D. degree in Earth, environment, and resources sciences.

His research interests include potential field modeling; multiscale potential field analysis; and joint inversion of geophysical datasets.

**Mojtaba Tavakoli** received the M.S. degree in geophysics and the Ph.D. degree in mining exploration from the Shahrood University of Technology, Shahrood, Iran, in 2013 and 2021, respectively.

He is working with the National Iranian Gas Company and as a Research/Teaching Assistant with the Shahrood University of Technology. His general research interests include is inversion of geophysical data, with focus on joint inversion approach.

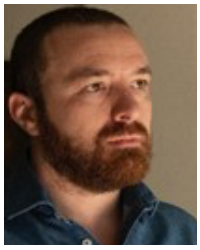

**Andrea Vitale** received the M.S. degree in geophysics and applied geophysics and the Ph.D. degree in Earth, environment, and resources sciences from the University of Naples Federico II, Naples, Italy, in 2014 and 2019, respectively.

He was a Post-Doctoral Research Fellow with the DiSTAR, University of Naples Federico II, from 2019 to 2020, and the CNR-IREA, Naples, from 2022 to 2023. His research interests include inversion of potential field data for exploration and monitoring purposes; application of AI to geosciences; Unmanned Aircraft Systems (UAS) for applied geophysics and its application for agriculture.

**Maurizio Fedi** received the M.Sc. degree in physics and the Ph.D. degree in applied geophysics from the University of Naples Federico II, Naples, Italy, in 1982 and 1987, respectively.

He was a Researcher with the University of Naples Federico II, from 1990 to 1992, and an Associate Professor with the University of Lecce, Lecce, Italy, from 1992 to 1996, and the University of Naples Federico II, from 1996 to 2000. He was a Visiting Professor with The University of British Columbia, Vancouver, Canada, the China University of Geosciences, Beijing, China, the National Geophysical Research Institute (NGRI), Hyderabad, India, the University of Tehran, Iran, and the China University of Geosciences, Wuhan, China. He has been a Full Professor with the Department of Earth, Environmental and Resource Science, University of Naples Federico II, since 2000. He is the author of more than 250 articles in international scientific journals and books. His research interests include potential field inversion and imaging, multifractal analysis, developments of interpretation techniques for dc resistivity, ground penetrating radar, frequency domain electromagnetic, and controlled source electromagnetic methods, integrated fields, and modeling geophysics.

Dr. Fedi was awarded the EGU Christiaan Huygens medal in 2023. He is also the Co-Editor-in-Chief of the *Journal of Applied Geophysics (Elsevier).*

Open Access funding provided by 'Università degli Studi di Napoli "Federico II"' within the CRUI CARE Agreement